Electric Power Systems Research 252 (2026) 112349

Contents lists available at ScienceDirect

Electric Power Systems Research

journal homepage: www.elsevier.com/locate/epsr

Hybrid WbOA–APINN framework for sustainable and intelligent energy management in renewable microgrids with hybrid energy storage

Jegadeesh Kumar R [a,*], Vijayakumar P [b], Santhosh Paramasivam [c,*], Amit Kumar [c], Gianluca Gatto [c]

[a] Department of Electronics and Communication Engineering, Rathinam Technical Campus, Coimbatore 641021, India
[b] Department of Electronics and Communication Engineering, PSG Institute of Technology and Applied Research, Coimbatore 641062, India
[c] Department of Electrical and Electronic Engineering, University of Cagliari, Cagliari 09123, Italy

ARTICLE INFO

Keywords:
Energy management system (EMS)
Renewable-integrated microgrids
Hybrid energy storage system (HESS)
Wombat optimization algorithm (WbOA)
Physics-informed neural network (PINN)
Smart grid optimization
Sustainable power systems
Low-carbon energy management

ABSTRACT

Energy management (EM) in renewable-integrated microgrids (MGs) with hybrid energy storage systems (HESS) is critical for ensuring operational reliability, reducing emissions, and minimizing costs. However, existing approaches often suffer from limited adaptability under dynamic conditions, reduced predictive accuracy, and insufficient renewable utilization. To overcome these limitations, this paper suggests a hybrid framework that integrates the Wombat Optimization Algorithm (WbOA) with an Augmented Physics-Informed Neural Network (APINN). In this framework, WbOA performs optimal scheduling of power distribution and charge–discharge operations of the HESS, while APINN enhances forecasting accuracy by embedding physical constraints such as power balance and storage dynamics into the learning process. Simulation results demonstrate that the suggested WbOA–APINN method outperforms benchmark techniques including PSO, GA, and recent hybrid models. Specifically, it achieves a system efficiency of 98.7 %, delivers 4.38 kWh of useful energy to the load over a 24-h horizon, reduces CO_2 emissions to 0.15 kg/kWh, and lowers operational cost to $124.5 per day by accounting for grid purchase, non-renewable generation, O&M, and battery degradation costs. These improvements highlight the synergistic benefits of integrating WbOA with APINN, offering a robust, scalable, and economically viable solution for intelligent EM in renewable-integrated MGs.

1. Introduction

1.1. Background

EM in MGs integrated with renewable energy sources (RESs) and HESSs plays a crucial role in enhancing power reliability, reducing dependence on conventional energy sources, and supporting environmental sustainability [1,2]. As the global energy demand continues to grow, integrating RESs such as solar as well as wind into MGs helps in utilizing locally available clean energy while minimizing transmission losses [3]. Nevertheless, renewable sources have the disadvantage of being intermittent and variable, which means that they can challenge the stable supply of power. To manage such variations, HESSs, which integrate technologies such as batteries as well as Supercapacitors (SCs) are implemented to balance energy in the short-term and the long-term [4,5]. With this setup, efficient EM demands that the generation, storage as well as consumption of power should be scheduled and managed optimally in relation to the dynamic load requirements. This is because the power flow (PF) is maintained by the inter- RESs coordination and storage units even when both the generation and demand are Variable [6,7]. With such systems, it can also be made to operate the MG in grid-connected and islanded modes which allows it to be more flexible and resilient in its operations [8]. Monitoring of the charging and discharging of storage devices based on the energy availability as well as demand helps in reducing wastage of energy and also increasing the life span of storage devices [9]. EM can also aid in peak shaving and load levelling which decreases the stress on the grid and the costs of operation. The use of the combination of RESs and HESSs in MGs helps to meet the goals of emission reduction by eliminating the use of fossil fuels as much as possible [10,11]. It also promotes energy independence in isolated and rural areas where people are not so reliant on central power. A properly scheduled EM plan may facilitate priority of loads, whereby the most important services are not interfered during the occurrence of a power shortage [12]. In addition, the operators can

* Corresponding authors.
E-mail addresses: jegadeeshkumar.eee@gmail.com (J.K. R), santhosh.paramasivam@unica.it (S. Paramasivam).

https://doi.org/10.1016/j.epsr.2025.112349
Received 18 August 2025; Received in revised form 6 October 2025; Accepted 6 October 2025
Available online 10 October 2025

better plan their maintenance and resources allocation based on forecasting energy generation and consumption trends. Last but not least, regulatory frameworks and incentive schemes are put in place to promote such sustainable energy infrastructures [13,14]. Power electronics and control systems develop MG component regulation. In general, EM in MGs including RESs and HESSs plays a crucial role in realizing sustainable, reliable, and affordable power systems [15].

1.2. Literature survey

Various studies have invested their research into EM in MGs integrated with RESs and HESS by applying different technological methods. This section reviews several research studies about EM in MGs integrated with RESs and HESS.

Sathishkumar et al. [16] have presented that hybrid PDO-MACNN algorithm to manage grid-independent hybrid RESs power in a HESS. To minimalize Total Harmonic Distortion (THD), provide active power balance by means of controlled charging as well as discharging and keep DC-link voltage within predefined operating limits, the method involves MACNN to forecast RESs performance and PDO to optimize three-phase inverter controller parameters. Ramu et al. [17] have introduced that an ANN based EM strategy to operate a DC MG system supported by a HESS and charged by a PV system. The HESS incorporates a battery and a SC so that they can exchange energy in a coordinated way, though using a Bidirectional Converter (BC). The ANN-based control was to stabilize the State-of-Charge (SoC), balance the loads, guide the PF and improve the voltage profile of the MG with various PV generation conditions. Kumar et al. [18] have presented that an intelligent MG including RESs and an energy storage system (ESS) applies the hybrid FFO-DADRCNN methodology of EM. The DADRCNN was applied to the accurate prediction of the load, as well as the FFO component was applied to regulate the MG system. By incorporating PV units, Wind Turbines (WTs), storage elements, and variable loads, this method aims at enhancing grid stability and operational performance and effectively managing load demand. Chekira et al. [19] have presented that an EM System (EMS) of an MG including variable load requirements, a HESS composed of batteries and SC, hybrid RESs (PV/ WT). The EMS uses an ANN-based system control system with Nonlinear Autoregressive Moving Average Level 2 (NARMA-L2) and a Maximum Power Point Tracking (MPPT) algorithm based on Nonlinear Autoregressive with exogenous inputs (NARX) in the PV system. Energy was distributed under the control of decision logic which takes account of battery SoC, available PV/WT power and load requirements. SCs reduce DC bus voltage excursions to enhance system stability and lifetime as well as reduce battery stress. Sruthi et al. [20] have introduced that RESs hybrid MRA-FLC approach to EM in DC MGs that support Electric Vehicle (EV) charging systems. The introduced solution reduces the wear and tear of storage devices and ensures the consistent power supply since the RESs were coupled with a Battery ESS (BESS). Srikanth et al. [21] have developed that CNNs were used to achieve SoC balancing through learnt nonlinear mappings between inputs and control actions in a centralized electromagnetic system for MGs with hybrid PV and BESS distributed generators. The CNN-based EMS performs better by optimizing the CNN weights using an ECOA, which eliminates the need for intricate computations. This approach learns from operational trends to provide accurate MG dynamics prediction and efficient control. Alghamdi [22] have introduced that the Improved Gradient-Based Optimization (IGBO) approach, which integrates RES and non-RESs in an MG with effective EM and scheduling using an IGBO algorithm. By controlling energy exchange with the grid and maximizing BESS charge-discharge cycles, the technique aims to optimize the use of RESs while reducing operating expenses. Kumar and Karthikeyan [23] have presented that the Golden Jackal Optimization (GJO) method, which could be used in EM in distributed-generation systems comprising hybrid RESs and BESS. To certify effective MG operation, the strategy aims at minimizing operating expenses and addressing constraints like power balance, generating constraints, and load requirement as well as the charge-discharge characteristics of storage units.

An improved EMS for a hybrid PV-WT MG with grid connectivity and battery storage was demonstrated by Merabet et al. [24]. The method incorporates load shifting to lower costs, investigates various profiles to enhance performance, optimizes battery power based on grid electricity pricing using a contribution factor, and takes component efficiencies into consideration when calculating energy costs. Hai et al. [25] an effective strategy for MG operation by integrating vehicle-to-grid (V2G) technology with RES. To address uncertainties in EV Charging (EVC) as well as discharging, renewable generation, load demand, and market price variations, the unscented transform (UT) was employed. The operational problem was formulated as a constrained single-objective optimization model with the goal of reducing total MG operational costs while meeting system constraints. To solve this, a modified marine predator algorithm (MMPA) was introduced as a robust as well as efficient optimization technique. To improve the EMS of DC MGs with incorporated EVs as well as PV production, Manikandan et al. [26] introduced PO-QSANN, a hybrid technique that combines Parrot Optimizer (PO) with Quantum Self-Attention Neural Networks (QSANN). The technique reduces costs and enhances efficiency via DC bus stabilization, optimized PI control, and quantum-inspired load prediction. An intelligent EMS based on a variety of RESs was given by Gaitan et al. [27]. A flexible EMS constructed by combining various RESs and energy storage (ES) facilities was referred to as an intelligent EMS. The goal was to provide a way to incorporate tiny energy sources to act like higher-power energy sources in order to maximize the usage of energy potential from renewable sources. Three RESs were included in the system that was introduced: solar, wind, also hydro. For a smart DC-MG, Belkhier et al. [28] have demonstrated an intelligent EM control technique based on a combination of fuzzy logic controller (FLC) methods and a modified super twisting algorithm (MSTA). The DC-MG integrated a hybrid energy source of battery, wind, and photovoltaic (PV). An intelligent MSTA managed source-side converters to prioritize RESs, maximize power, and ensure stable, high-quality output efficiently. Using a Raspberry Pi microcontroller, Carrasco-Gonzalez et al. [29] have demonstrated the design and implementation of a unique intelligent EMS for a grid-connected hybrid MG (HMG) with AC and DC MGs. The DC MG incorporates DC loads, a WT, an ultracapacitor (UC), as well as a hydrogen system. In the meanwhile, the AC MG consists of a PV generator, three-phase loads, and a battery bank. Each device in the HMG was controlled by a local controller, and all of the devices were regulated by a dynamic FLC-based EMS that was implemented on a Raspberry Pi microcontroller. A new multi-objective optimization (MOO) model for designing and improving a Renewable Integrated Energy System (RIES) that integrates RESs, ES technologies, and energy sharing mechanisms has been presented by Shafiei et al. [30]. The approach combines a MOO framework with gravity search algorithm (GSA) to enhance resilience, cut carbon emissions, and boost economic benefits, while integrating ES and renewable energy (RE) to minimize energy losses as well as balance supply with demand. Comparative analysis of methods EM in MGs integrated with RESs and HESS is illustrated in Table 1.

1.3. Research gap and contributions

Although several methods have been suggested for EM in MGs integrated with RESs and HESS, significant gaps remain. Approaches such as PDO-MACNN focus on reducing harmonic distortion and stabilizing the DC-link voltage, but they lack adaptability to dynamic load and generation conditions. ANN-based methods emphasize SoC preservation and voltage control but fall short in predictive accuracy for highly variable renewable outputs. Hybrid techniques like FFO-DADRCNN improve load prediction and control but do not sufficiently address emission reduction or renewable utilization. Similarly, strategies such as NARX–NARMA-L2 and MRA-FLC manage resource coordination but fail

Table 1
Comparative analysis of EM techniques in MGs integrated with RESs and HESS.

Refs.	Methodology	System Configuration	Key Focus / Contribution	Limitations
Sathishkumar et al. [16]	PDO-MACNN	Grid-independent hybrid RESs with HESS	Forecasts RESs performance and optimizes inverter parameters to minimize THD and maintain DC-link stability.	Limited adaptability under highly uncertain RESs and nonlinear load changes.
Ramu et al. [17]	ANN	DC MG with PV, Battery + SC	Stabilizes SoC, balances PF, and manages DC voltage profile under varying PV generation.	Performance degrades under abrupt load fluctuations or faulty sensors.
Kumar et al. [18]	FFO-DADRCNN	Smart MG with PV, WT, Storage	Enhances load prediction and operational control for grid stability.	High computational burden; prediction accuracy highly dependent on data quality.
Chekira et al. [19]	NARX + NARMA-L2 ANN	MG with PV/WT and HESS (Battery + SC)	Combines MPPT with decision logic for energy scheduling under variable loads.	Complex tuning; limited generalization to unseen load patterns.
Sruthi et al. [20]	MRA-FLC	DC MG with RESs and Battery (EVC support)	Manages PF to reduce storage degradation and support consistent EVC.	May not scale well to large or highly dynamic MGs.
Srikanth et al. [21]	CNN-ECOA	Centralized EMS for MG with PV + Battery	Learns nonlinear mappings for efficient SoC balancing without detailed system modelling.	Requires substantial training data and lacks decision transparency.
Alghamdi [22]	IGBO	MG integrating RESs and non-RES	Effective scheduling and cost minimization through hybrid RESs and BESS coordination.	Limited scalability and slower convergence for larger MGs.
Kumar & Karthikeyan [23]	GJO	Distributed Generation MG with RESs + BESS	Cost reduction with constraint handling under EM objectives.	Sensitive to initial parameter settings and heuristic biases.
Merabet et al. [24]	Parameter-based EMS	Hybrid Solar-Wind MG with Battery Storage and Grid Connection	Contribution factor-based battery power allocation depending on grid price; load shifting for cost reduction.	Limited forecasting under high uncertainty.
Hai et al. [25]	MMPA	MG with V2G and RES	Tackles uncertainties in EV, renewable generation, load, and market price variations for cost minimization.	Single-objective optimization limits multi-criteria performance.
Manikandan et al. [26]	PO-QSANN	DC MG with PV and EVs	Stabilizes DC voltage, reduces operating cost, improves load prediction accuracy via quantum attention.	Computational complexity and large training data requirements.
Gaitan et al. [27]	Intelligent EMS with multiple RES	Standalone hybrid system with solar, wind, hydro + batteries & hydro basin storage	Increases renewable utilization by integrating small-scale RESs into a higher-capacity source; flexible EMS for standalone operation.	No grid connection; limited scalability for urban applications.
Belkhier et al. [28]	MSTA + FLC	Smart DC-MG with PV, Wind, Battery bank	Controls source-side converters to maximize renewable power extraction, ensure smooth power, and prioritize RESs to reduce cost.	Controller design complexity; performance sensitive to parameter tuning.
Carrasco-Gonzalez et al. [29]	Fuzzy Logic EMS on Raspberry Pi	Grid-connected hybrid MG with AC and DC subsystems (PV, WT, hydrogen, battery, UC)	Implements fuzzy EMS with local controllers for multi-device coordination; validated against conventional EMS.	Processing limitations of Raspberry Pi may restrict large-scale applications.
Shafiei et al. [30]	GSA-based MOO	RIES with RES, storage, energy sharing	Enhances resilience, carbon reduction, and economic benefit; minimizes losses through optimal integration.	Complexity increases with larger-scale multi-objective formulations.
This Work (Proposed)	WbOA-APINN	Grid-connected MG with PV, WT, Battery, and SC (HESS)	Optimizes PF and forecasts renewable generation and load to reduce cost, emissions, and improve efficiency.	Fixed emission factor; does not consider real-time market price dynamics.

to quantify their overall impact on efficiency. CNN-ECOA improves SoC balancing but remains limited in adaptability under fluctuating conditions, while IGBO and GJO primarily target cost optimization without validating performance under high renewable penetration and emission constraints. The restrictions point to the necessity of more powerful solutions that would result in less energy consumption, less emission, more efficiency, and proper integration of renewable in active environments. In order to address these issues, this paper suggests the WbOA-APINN method of intelligent EM in renewable-integrated MGs. The WbOA can optimize the power distribution and charge-discharge timetable of the HESS, whereas the APINN generates the realistically accurate forecasts of the renewable production and load necessities. Collectively, they create a synchronized optimization-forecasting system that would provide efficient scheduling, cost-saving, emission-reduction, and used RE more effectively.

The choice of WbOA over more established metaheuristics like Particle Swarm Optimization (PSO), Genetic Algorithm (GA), or Whale Optimization Algorithm (WOA) is deliberate. WbOA provides a better trade-off between exploration and exploitation by way of its tunnelling and foraging functions, making it is able to escape early convergence and reach stable solutions in nonlinear and constrained scheduling issues. In combination with APINN, which entails physical constraints of the prediction process, the synergy here is clear: WbOA is used to generate high quality globally optimized scheduling decisions, whereas APINN is focused on attaining predictive accuracy in the presence of varying renewable and demand conditions. This iterative integration transcends beyond an incremental integration of already existing methods to provide a single optimization-prediction framework specific to renewable-integrated MGs.

The following is a summary of this work's contributions:

- The WbOA-APINN approach is suggested for EM in MG systems integrated with RESs and HESS.
- WbOA is utilized to optimize power distribution and the charge–discharge scheduling of HESS components, ensuring efficient resource utilization.
- APINN is utilized to accurately predict RE generation and load demand, supporting proactive control decisions.
- The integration of WbOA and APINN enhances EM by minimizing energy consumption, emissions, and operational cost while improving system efficiency and increasing RE utilization.

The novelty of this approach lies in combining WbOA's optimization capability with APINN's physics-informed predictive modelling. Unlike existing methods, the suggested technique embeds system dynamics into the learning process, enabling adaptive and accurate control strategies. This enhances renewable utilization, reduces operational costs and emissions, and ensures reliable and efficient MG operation under

varying conditions.

The remainder of this work is structured as follows: Part 2 explains the configuration of the MG integrated with RESs and HESS. Part 3 presents the cost reduction strategy using the WbOA-APINN technique. Part 4 discusses the results and discussion. Part 5 concludes the manuscript.

2. Configuration of microgrid system integrated with RESs and HESS

Fig. 1 demonstrates the detailed design of a MG system that combines RESs and a HESS to ensure reliable as well as sustainable energy supply. The RESs consist of WTs and PV panels, both of which are responsible for harnessing RE from natural sources and converting it into DC power using respective dedicated converters. These DC outputs are then connected to a central AC/DC converter interface, allowing bidirectional PF between the generation sources, the load, and the utility grid. This configuration enables the system to either feed surplus energy into the grid or draw from it when required. To address the variability and intermittency of RESs, a HESS is incorporated, consisting of a BESS and a SC. Both storage units are connected to the DC bus through their own converters, which manage the charge and discharge processes independently and efficiently. The suggested WbOA-APINN technique governs the EM by optimizing power distribution and HESS scheduling using the WbOA, while the APINN predicts renewable generation and load demand to support efficient decision-making across the system.

2.1. Modelling of wind

The mechanical power extracted by a WT is governed by the kinetic energy of the wind flowing through the rotor swept area and is expressed as [31]:

$$P_m(t) = \frac{1}{2}\rho C_P(\lambda, \beta) A V_t^3 \tag{1}$$

Where ρ denotes air density, A indicates swept area of the blades, C_P represents power coefficient depending on tip-speed ratio λ and pitch angle β.

The practical electrical output power of a WT is determined by its cut-in, rated, and cut-off wind speeds (WS). It can be expressed as:

$$P_{WT}(t) = \begin{cases} 0 & V(t) \le V_{cin} \text{ or } V(t) \ge V_{coff} \\ P_R^W \dfrac{V(t) - V_{cin}}{V_R - V_{cin}} & V_{cin} < V(t) < V_R \\ P_R^W & V_R \le V(t) < V_{coff} \end{cases} \tag{2}$$

where V_{cin},V_R, and V_{coff} are the cut-in, rated, and cut-off WS, respectively, and P_R^W is the rated power of the WT. A probability density

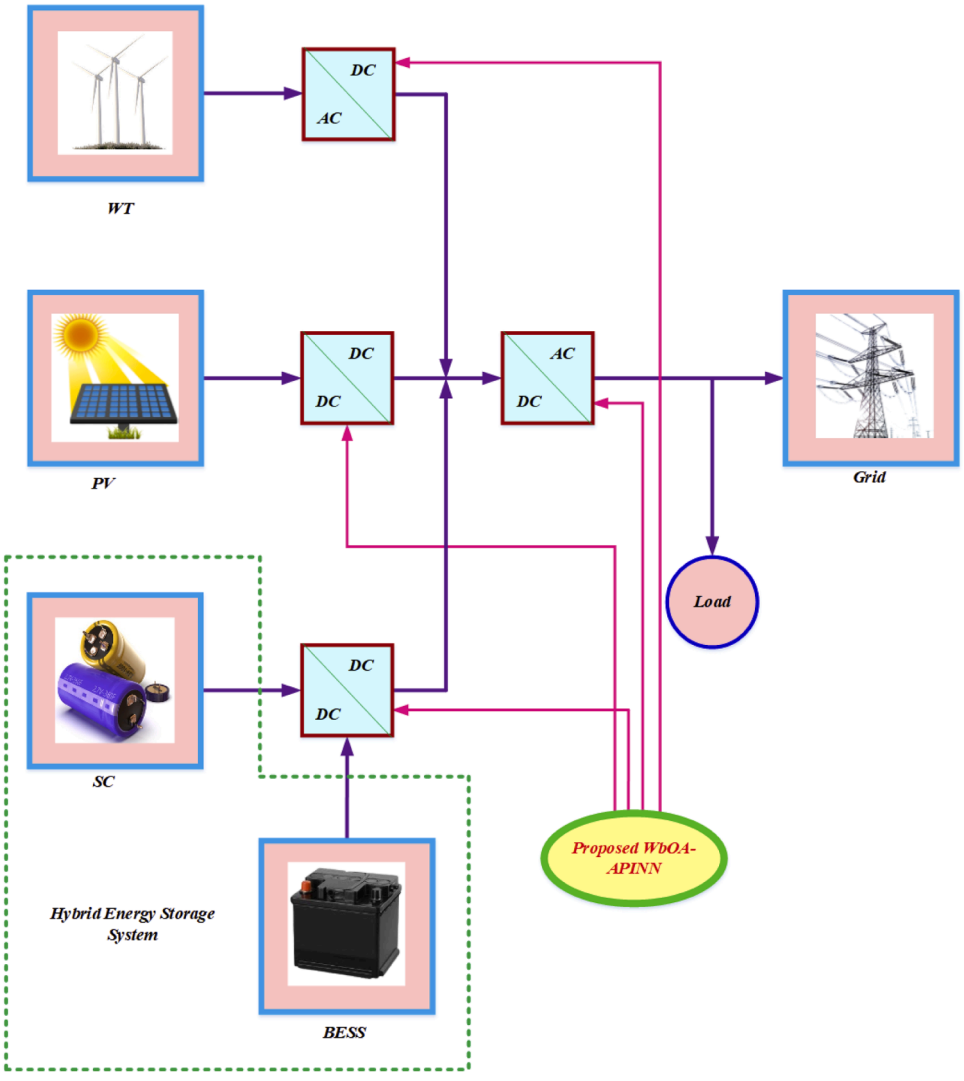

Fig. 1. Structure of MG system integrated with RESs and HESS.

function (PDF) is a curve that shows WS over the course of the year.

$$P(v_1 \le v \le v_2) = \int_{v1}^{v2} F_v \, dv \tag{3}$$

$$P(0 \le v \le \infty) = \int_{v1}^{\infty} F_v \, dv = 1 \tag{4}$$

Where F_v represent the WS PDF, v_1 and v_2 represent the any 2 WS. The Weibull probability function, which forms the basis for explaining WS statistics, is defined as follows:

$$F_v = \frac{K}{C}\left(\frac{v}{C}\right)^{K-1} \exp\left(\left(\frac{v}{C}\right)^{K}\right) \tag{5}$$

where, K, C and v stand for the shape parameter, scale parameter, and WS, respectively. The following formula can be used to get the WS at a given height:

$$V = V_0 \left(\frac{E_{WT}}{E_0}\right)^{\alpha} \tag{6}$$

where the WS at the required height is represented by V, V_0 and α. The friction coefficient is denoted by E_0, and the WS at reference height by E_{WT}.

$$P_{WT}(t) = M_{WT} P_{WT}(t) \tag{7}$$

where M_{WT} represent the number of WT.

2.2. Modelling of SC

In addition to the BESS, a SC is integrated into the HESS of the MG. The SC is chosen due to its complementary characteristics compared to batteries. It provides high power density, rapid charge-discharge capability, and a long cycle life, making it ideal for managing short-term power fluctuations in renewable generation and load demand. Specifically, the SC is used to handle sudden power surges or drops, absorbing excess energy during renewable generation peaks and providing power during short-term high load demands. This approach reduces the stress on the battery system, improves the overall EM efficiency, and significantly extends the battery's lifespan. Unlike large-scale applications that typically use hydro-pumped storage for bulk EM, SCs are more suitable for distributed, small- and medium-scale MG applications where space is limited and fast response is required. SCs are among the newest advancements in power storage technology, especially in integrated systems [32]. In this setup, a capacitance $(c_{supercapacitor})$ is connected to an analogous series resistance $(r_{supercapacitor})$. The SC voltage $(v_{supercapacitor})$ as a function of the SC current $(i_{supercapacitor})$ is calculated using the formula below:

$$\begin{aligned} v_{supercapacitor} &= v_1 - r_{supercapacitor} \times i_{supercapacitor} \\ &= \frac{q_{supercapacitor}}{S_{supercapacitor}} - r_{supercapacitor} \times i_{supercapacitor} \end{aligned} \tag{8}$$

Where, $q_{supercapacitor}$ indicates quantity of electricity present in the cell. The power of SC $p_{supercapacitor}$ is determined using Eqn (8)

$$p_{supercapacitor} = \frac{q_{supercapacitor}}{c_{supercapacitor}} \times i_{supercapacitor} - r_{supercapacitor} \times i^2_{supercapacitor} \tag{9}$$

2.3. Modelling of PV

The best design of a solar PV cell depends on modelling, which raises the PV system's overall performance. Any PV system's behaviour in real time can be efficiently mirrored by a precise and comprehensive PV cell model. However, the cell's intrinsic nonlinearity, modelling PV cells can be difficult [33]. The total current produced by the single-diode PV model is shown by the following expression:

$$I = I_{PV} - I_d - I_P \tag{10}$$

where I_{PV} indicates the current produced by the PV, I_d indicates the current passing through the diode, and I_P indicates the current through the shunt resistance. With the substitution of I_d and I_P, the present equation can be expressed as follows:

$$I = I_{PV} - I_0\left(\exp\left(\frac{V_d}{q_1 V_t} - 1\right)\right) - \left(\frac{V + IR_S}{R_P}\right) \tag{11}$$

where V_t denotes the thermal voltage, q_1 indicates ideality factor, I_0 represent the diode d is the diode leakage current and R_S indicates the number of cells linked in series. A PV system's power output is largely influenced by its surroundings. Therefore, the following formula can be used to represent the current produced by a PV source mathematically:

$$I_{PV} = \left(\frac{g}{g_0}\right)\left[I_{SC} + K_j(T - T_0)\right] \tag{12}$$

where I_{SC} denotes the short-circuit current under standard test conditions, the current coefficient factors are represented by K_j, while the actual temperature and irradiation values are denoted by g and T, respectively. The cell temperature in Kelvin is indicated by T, and the Boltzmann constant is represented by K.

2.4. Modelling of battery storage

The BESS is modelled using standard energy balance equations to track the SoC at each time step during charging and discharging [34]. The equations are given by:

$$SoC(t) = SoC(t-1) \times (1 - \sigma_{bat}) + \frac{p_b(t) \times \eta_{Sys\_b} \times \Delta t}{n_B \times c_{Sys\_Unit}} \tag{13}$$

$$SoC(t) = SoC(t-1) \times (1 - \sigma_{bat}) - \frac{p_b(t) \times \eta_{Sys_b} \times \Delta t}{n_B \times c_{Sys_{Unit}}} \tag{14}$$

Where $p_b(T)$ represents the battery power at all times T, $SoC(T)$ the level of charge of the system battery at any time T, σ_{bat} the self-discharge rate of the storage battery, and η_{Sys_b} the effectiveness of the storage battery's charging and discharging. To increase the lifespan of the storage battery, it should not be overcharged or over discharged. Stated otherwise, the storage battery's SoC must remain within the specified bounds at all times T:

$$SoC_{MIN} \le SoC(t) \le SoC_{MAX} \tag{15}$$

where SoC_{MIN} and SoC_{MAX} denotes the storage battery's minimum and maximum permitted SoC, respectively.

2.5. Power converter modelling

The greatest predictable power of loads ($Power^{Max}_{Load}$) should be supported by a converter [35]. As a result, the inverter efficiency (η_{inv}) is used to estimate the inverter rated power ($Power_{inv}$) as follows:

$$Power_{inv} = \frac{Power^{Max}_{Load}}{\eta_{inv}} \tag{17}$$

2.6. AC grid modelling

The AC grid converter system's mathematical modelling can then be expressed as follows [36].

$$\frac{Dv_G}{DT} = \frac{i_G}{c_G} - \frac{i_{l_G}}{c_G} \tag{18}$$

$$\frac{v_G}{l_G} = \frac{Di_G}{DT} + (1-u)\frac{v_{DC}}{l_G} - d_1 \tag{19}$$

$$\frac{Dv_{DC}}{DT} = (1-u)\frac{i_{l_G}}{c_{DC}} - \frac{i_{o_G}}{c_{DC}} + d_2 \tag{20}$$

Where, $i_G$refers rectified current of grid, $v_G$refers grid rectified input voltage, $u$indicates controller signal, $d_1$and $d_2$indicates dynamical uncertainty in the parameters of the energy stage, i_{l_G} indicates current of the inductor, c_{DC}indicates DC-link capacitor.

2.7. Objective function (OF)

The CO_2 emissions are computed using the following equation:$CO_2\,Emissions = \sum_{t=1}^{k} \omega_{CO_2} \cdot E_{CO_2}(t)$ (21)

Where, ω_{CO_2} denotes weighting factor or emission factor for CO_2 in kg, $E_{CO_2}(t)$ represents energy generated from non-renewable sources at time step t, and k indicates total number of time steps.

The system efficiency is calculated using the following equation:

$$\eta_{system} = \frac{\sum_{t=1}^{k} p_{load}(t) \times \Delta t}{\sum_{t=1}^{k} \left[P_{pv}(t) + P_{WT}(t) + P_{Grid}(t)\right] \times \Delta t} \tag{22}$$

Where, $p_{load}(t)$ represents power supplied to the load, $P_{pv}(t)$ denotes power generated by PV units, $P_{WT}(t)$ is power generated by WTs, $P_{Grid}(t)$ denotes power imported from the grid, and Δt represents time interval of the simulation.

The reported energy consumption is now presented as the total energy delivered to the load during the simulation period, in kilowatt-hours (kWh):

$$E_{consumed} = \sum_{t=1}^{k} P_{load}(t) \times \Delta t \tag{23}$$

The equation used to compute the operational cost is as follows:

$$C_{operational} = \sum_{t=1}^{k} \left[P_{Grid}(t) \times C_{grid} + P_{non-res}(t) \times C_{non-res} + C_{O\&M} + C_{\deg}\right] \times \Delta t \tag{24}$$

Where, $P_{Grid}(t)$ is power imported from the grid, $P_{non-res}(t)$ represents power generated by non-renewable sources, C_{grid} denotes grid electricity price, $C_{non-res}$ represents non-renewable generation cost, $C_{O\&M}$ is fixed operation and maintenance cost per time interval, and $C_{\deg}$ denotes battery degradation cost.

3. Cost reduction of MG system integrated with RESs and HESS based on WbOA-APINN technique

Minimization of energy consumption, emissions, and operational cost, along with the enhancement of efficiency and renewable utilization in MG systems integrating RESs and HESS, is the main focus of this study. The proposed WbOA-APINN framework combines metaheuristic optimization with physics-informed forecasting. WbOA optimizes power distribution and HESS scheduling, while APINN predicts renewable generation and load demand profiles with high accuracy under uncertainty. This dual approach ensures that scheduling decisions are both optimized and supported by physically consistent forecasts. The following subsections provide a detailed description of the WbOA optimization and APINN prediction components.

3.1. Optimization using WbOA technique

The WbOA is a bio-inspired metaheuristic algorithm modelled on the burrowing and foraging behaviours of wombats [37]. In this approach, each wombat (wb) represents a potential solution to the EM problem, with its "position" corresponding to a candidate scheduling and power allocation strategy. The algorithm operates through two alternating phases. During the exploration, or foraging phase, candidate solutions survey wide regions of the search space, emulating Wbs scanning large habitats for food. This mechanism helps prevent premature convergence to suboptimal schedules. In the exploitation, or tunnelling phase, candidate solutions concentrate on promising regions, refining charge–discharge schedules by focusing on high-fitness areas. This ensures convergence toward near-optimal strategies. The careful balance between exploration and exploitation makes WbOA particularly well-suited for MG EM problems, which are characterized by nonlinearities, operational constraints, and fluctuating inputs. The detailed procedural steps of WbOA are described as follows.

Step 1: Initialization

Input parameters such as solar irradiance, WS, battery SoC, and power levels of SC and battery are initialized.

Step 2: Random Generation

Random vectors generate multiple candidate solutions, ensuring diversity in initial configurations of power distribution and HESS scheduling. This increases the chances of finding global optima.

Step 3: Fitness Function

Evaluate the fitness value of each candidate solution based on criteria such as minimized operation cost of the system.

$$F = \min\left(C_{operational} + CO_2\,Emissions\right) \tag{25}$$

Where, Fdenotes fitness function.

Step 4: Exploration

The location of the Wb in the problem-solving space undergoes an update during the first phase of WbOA based on its foraging behaviour modelling. The herbivorous Wb organically traverses over an extensive portion of its habitat in search of sustenance because of its proficient searching capacity. The Wbs scans broad regions for viable EM strategies.

Eq. (26) is used to determine each Wb's set of foraging sites.

$$Cfp_j = \{Y_i : f_i\, and\, i \neq j\} \tag{26}$$

Where, Cfp_j denotes the set of possible foraging positions for the j^{th} Wb, Y_i denotes a population member with a higher OF value than the j^{th} Wb, and f_i denotes the OF value.

It is assumed in the design of WbOA that the Wb moves in the direction of one of these fodder positions at random. Each WbOA member has a new position determined by Eq. (27). Using if this new position increases the OF value, it replaces the previous position of the linked member, as per Eq. (24).

$$y_{j,k}^{p1} = y_{j,k} + R_{j,k} \cdot \left(Sfp_{j,k} - E_{j,k} \cdot y_{j,k}\right) \tag{27}$$

$$Y_j = \begin{cases} Y_j^{p1} & f_j^{p1} \leq f_j \\ Y_j & ELSE \end{cases} \tag{28}$$

Where, $Sfp_{j,k}$ indicates selected forage position for the j^{th} Wb, Y_j^{p1} denotes new position calculated for the j^{th} Wb, $y_{j,k}^{p1}$ denotes its j^{th} dimension, f_j^{p1} denotes its OF value, $R_{j,k}$ denotes random numbers from the interval [0, 1], $E_{j,k}$ denotes numbers which are randomly selected as 1 or 2.

Step 5: Exploitation

Wbs simulates tunnelling behaviour to evade predators, which metaphorically guides them to better local optima in energy scheduling. The Wb creates numerous tunnels in its territory because of its strong digging capabilities. Under threat from predators the Wb chooses to evade attack by plunging toward nearby tunnels to save itself.

New positions are computed based on neighbouring high-fitness zones, reflecting possible charge/discharge actions using of Eq. (29) during the positioning calculation process in the WbOA design

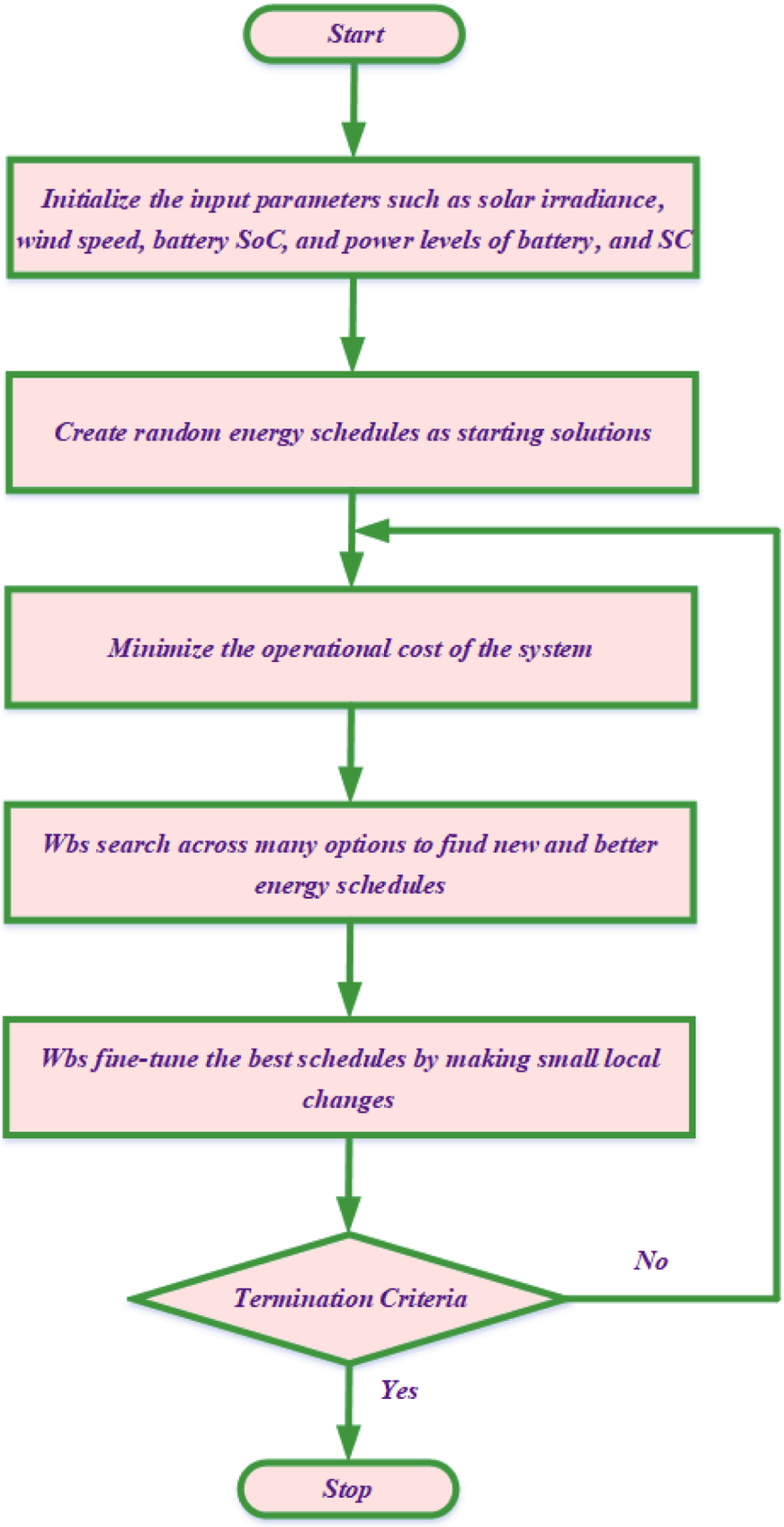

Fig. 2. Flowchart of WbOA.

framework. The Eq. (30) will replace the existing position of the member but only when the new position results in better OF value.

$$y_{j,k}^{p2} = y_{j,k} + (1 - 2R_{j,k}) \cdot \frac{Ub_k - Lb_k}{T} \tag{29}$$

$$Y_j = \begin{cases} Y_j^{p2} & f_j^{p2} \le f_j \\ Y_j & ELSE \end{cases} \tag{30}$$

Where, Y_j^{p2}denotes new position calculated for the j^{th} Wb based on the escape phase, $y_{j,k}^{p2}$denotes its j^{th} dimension, f_j^{p2}denotes its OF value, Tdenotes iteration counter.

Step 6: Termination

The process terminates either when the maximum number of iterations is reached or when improvements fall below a tolerance threshold for several iterations. This ensures computational efficiency without sacrificing accuracy. By iteratively updating solutions through these phases, WbOA identifies optimal scheduling strategies that balance renewable generation, HESS operation, and grid interaction. A flowchart of the process is shown in Fig. 2.

3.2. Prediction using APINN technique

In MGs, the APINN is used to forecast load demand profiles and RE generation [38]. Unlike conventional neural networks that rely purely on data, APINN incorporates physics-informed constraints into its learning process, ensuring that predictions adhere to the underlying physical laws governing energy flow. The technique employs soft domain decomposition, where a gating network partitions the input domain into sub-regions. Each sub-network then specializes in capturing localized patterns, such as midday solar peaks or evening load rises, which prevents overfitting and effectively models heterogeneous system behaviour. Additionally, APINN utilizes a physics-informed loss function that integrates boundary conditions, such as power balance constraints, residuals of governing partial differential equations (PDEs) describing renewable generation and load dynamics, and continuity losses to enforce smooth transitions across sub-networks. This combination ensures that the predictions remain consistent with both observed data trends and physical feasibility.

The output of the APINN model is defined by this Eqn (31).

$$v_\theta(z) = \sum_{i=1}^{m} (H(z))_i F_i(g(z)) \tag{31}$$

Where, $v_\theta(z)$ denotes predicted solution of the PDE, $(H(z))_i$is the gating function that assigns a weight to each sub network, $F_i(g(z))$ represents the sub network responsible for solving a sub domain and $g(z)$ is a shared network that extracts features from the input.

The total loss function of APINN is represented by the following Eq. (32).

$$P(\theta) = \frac{1}{m_b}\sum_{i=1}^{m_b} \left| v_\theta(z_{b,i}) - q(z_{b,i}) \right|^2 + \frac{1}{m_r}\sum_{i=1}^{m_b} \left| Lv_\theta(z_{r,i}) - f(z_{r,i}) \right|^2 \tag{32}$$

Where, $P(\theta)$ is the total loss used to train the network, m_b and $m_r$denotes number of boundary and residual points, respectively, $V_\theta(z_{b,i})$ is the predicted solution at boundary points, $q(z_{b,i})$is the known boundary condition,$Lv_\theta(z_{r,i})$ indicates PDE residual loss, $f(z_{r,i})$ indicates source term of the PDE.

The controlling PDE, which governs the physical behaviour of RE flow and demand, is expressed as Eq. (33):

$$Lv^*(z) = f(z), \quad v^*(z) = q(z) \ on \ \partial\Omega \tag{33}$$

Where, L is a differential operator applied to the solution,$v^*(z)$is the exact ground-truth solution, $f(z)$ is the external forcing function or source term, $q(z)$is the known boundary condition and $\partial\Omega$ represents the boundary of the solution domain.

The behaviour of the gating function, which blends contributions from sub-networks, is defined by Eq. (34):

$$(H(z,t))_1 = 1 - (H(z,t))_2 = e^{-t} \tag{34}$$

Where, $H(z,t)$determines how the sub networks contribute to the final solution, $(H(z,t))_1$and $(H(z,t))_2$are the weighting functions for two sub networks and e^{-t}ensures a smooth transition between subdomains.

Eq. (35) ensures smooth transitions between sub-networks, preventing abrupt changes in forecasts.

$$S_a(\theta_i, \theta_j) = \frac{1}{m_{I,ij}} \sum_{k=1}^{m_{I,ij}} \sum_{n=1}^{d} \left| \frac{\partial v_{\theta_i}(Z_{I,K})}{\partial z_n} - \frac{\partial v_{\theta_j}(Z_{I,K})}{\partial z_n} \right|^2 \tag{35}$$

Where, $S_a(\theta_i, \theta_j)$ denotes continuity loss function, $m_{I,ij}$ denotes number of interface points between sub networks $i$and$j$, $\frac{\partial v_{\theta_i}(Z_{I,K})}{\partial z_n}$ *and* $\frac{\partial v_{\theta_j}(Z_{I,K})}{\partial z_n}$represents the derivative of the predicted solution from sub network $i$and$j$. APINN effectively predicts RE generation and load demand profiles, thereby enabling improved scheduling, resource planning, and system operation in MG environments.

To ensure fairness in performance evaluation, all algorithms were tested under identical conditions. Table 2 summarizes the simulation setup.

The hyperparameters for each algorithm were carefully tuned to ensure fair comparison. WbOA used a population size of 30 with 500 iterations to balance convergence and runtime. APINN was trained with four hidden layers and ReLU activations, optimized using Adam. Competing methods such as MACNN and ANN were also configured with commonly accepted parameters for unbiased evaluation. These are summarized in Table 3.

4. Results and discussion

The performance of the suggested WbOA-APINN method for improving EM in MG systems integrated with RESs and HESS is demonstrated in this section through simulation results. This method aims to minimize energy consumption, emissions, and operational cost while enhancing efficiency and RE utilization by optimizing power distribution and HESS scheduling, and accurately predicting renewable generation and load demand. The approach has been implemented on the MATLAB, and its effectiveness in managing energy flow and system performance under varying operating conditions has been thoroughly evaluated and compared with existing methods.

Fig. 3 shows evaluation of solar radiance. The radiance pattern begins with 0 W/m^2 from 0 to 6 h, rises sharply after sunrise, and reaches nearly 250 W/m^2 at 9 h. The maximum value is observed at 12 h with 700 W/m^2, which then decreases symmetrically to 400 W/m^2 at 14 h and 100 W/m^2 by 17 h, finally dropping back to 0 W/m^2 after 18 h. This pattern reflects typical daily solar availability, with maximum energy

Table 2
Experimental setup and simulation environment used for all compared algorithms.

Category	Details
Software Environment	MATLAB R2020a
Toolboxes Used	Optimization Toolbox, Deep Learning Toolbox, Parallel Computing Toolbox
Solver	fmincon (constrained nonlinear optimization solver)
Simulation Horizon	24 h (86,400 time steps)
Simulation Time Step	1 s
Dataset & Constraints	Identical dataset and system constraints applied to all algorithms

Table 3
Hyperparameters of the suggested WbOA-APINN and benchmark algorithms.

Algorithm	Hyperparameters
WbOA	Population size = 30; Iterations = 500; Exploration–exploitation = random [0,1]
APINN	Hidden layers = 4; Neurons/layer = 64; Activation = ReLU; Learning rate = 0.001; Batch size = 128; Epochs = 200; Optimizer = Adam
MACNN	Conv. layers = 3; Kernel size = 3 × 3; Filters = 32, 64, 128; Activation = ReLU; Learning rate = 0.001; Optimizer = Adam
ANN	Hidden layers = 3; Neurons/layer = 64; Activation = Tanh; Learning rate = 0.005; Optimizer = SGD with momentum
PDO	Population size = 20; Iterations = 400; Inertia weight = 0.7; Acceleration constants = c1 = c2 = 1.5

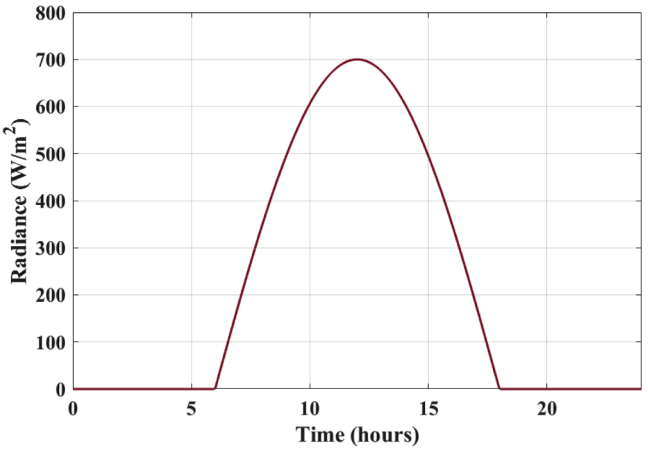

Fig. 3. Evaluation of solar radiance.

potential concentrated in midday hours. It directly drives PV generation, showing the critical dependency of renewable supply on natural conditions. Fig. 4 illustrates evaluation of WS. The WS starts very low at around 0.3 m/s during the first hour, increases gradually to 0.6 m/s at 4 h, and continues to rise to 1.5 m/s by 9 h. Between 10–12 h, it fluctuates around 1.7–1.9 m/s, before dropping slightly to 1.4 m/s at 15 h. Afterward, it shows a second growth phase, reaching 2.0 m/s at 20 h and peaking at 2.2 m/s around 21 h, before tapering slightly to 1.9 m/s by 23 h. These irregular fluctuations highlight the intermittent nature of wind resources, demonstrating the need for HESS to buffer variability and maintain supply stability. Fig. 5 denotes evaluation of WT power. The WT power output starts at about 0.8 kW at 1 h, increases gradually to 2.5 kW at 5 h, and further rises to 4.1 kW by 7 h. A noticeable surge is seen at

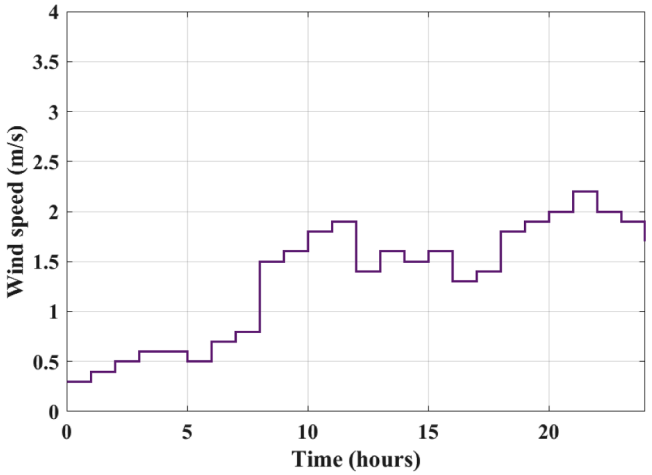

Fig. 4. Analysis of WS.

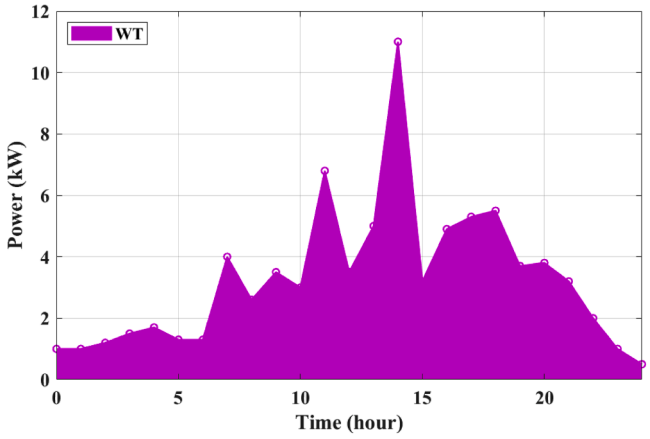

Fig. 5. Assessment of WT power.

11 h where output peaks at 6.8 kW, followed by fluctuations between 3.5–5.0 kW until 13 h. The highest generation occurs around 15 h with 10.8 kW, after which the power stabilizes at 4.5–5.5 kW from 16 to 20 h. Toward the end of the cycle, the values decline, reaching 2.2 kW at 22 h and about 0.6 kW by 23 h. Small changes in WS cause large swings in WT power due to cubic dependency, explaining the spikes observed. This underlines the importance of optimization in ensuring grid stability when relying on wind energy. Fig. 6 shows evaluation of grid power. The grid power remains steady at around 0 kW until 5 h, after which it starts oscillating significantly between −10 kW and +20 kW. From 6 to 16 h, the oscillations intensify, mostly fluctuating in the range of 5–18 kW with repeated peaks. After 17 h, the magnitude decreases slightly, with oscillations narrowing down to 3–10 kW. These exchanges balance renewable intermittency, with the proposed strategy ensuring grid dependency is minimized and controlled within safe bounds.

Fig. 7 implies evaluation of load power. The load demand begins at 0 kW at 0 h, then increases progressively to about 5 kW at 4 h, reaching 12 kW at 10 h. It further rises to 15 kW at 13 h and peaks at nearly 18 kW around 16 h. Afterward, the demand starts reducing, dropping back to 12 kW at 20 h, and ends close to 10 kW at 24 h. This daily cycle reflects realistic residential/industrial demand. Proper forecasting of this trend enables efficient scheduling of storage and renewable dispatch. Fig. 8 shows evaluation of PV power. The PV generation initiates at 0 kW until 6 h, increases steadily to 7 kW at 8 h, and reaches its maximum of about 15 kW around 11 h. After that, it decreases symmetrically, dropping to 10 kW at 13 h, 3 kW at 16 h, and finally to 0 kW after 18 h. The bell-shaped curve confirms model accuracy and highlights PV's role as the main daytime energy source. Its predictability makes it a stable

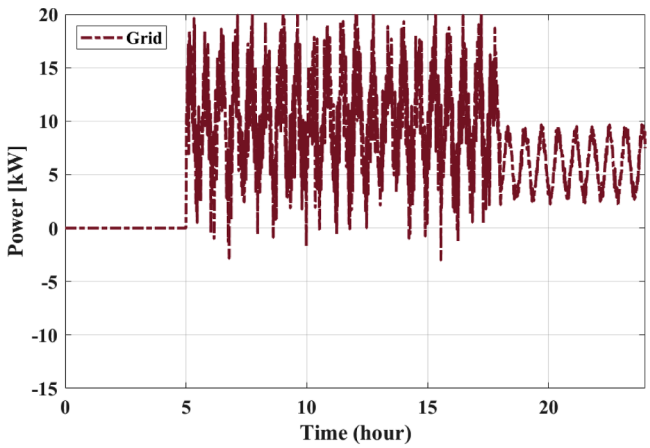

Fig. 6. Evaluation of grid power.

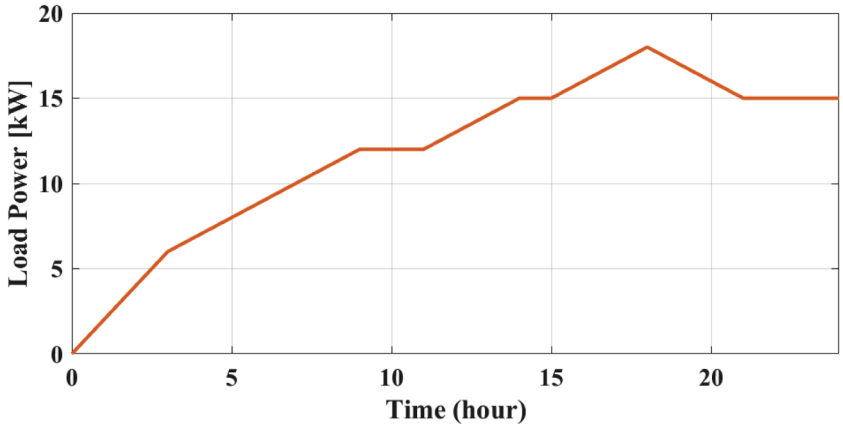

Fig. 7. Analysis of load power.

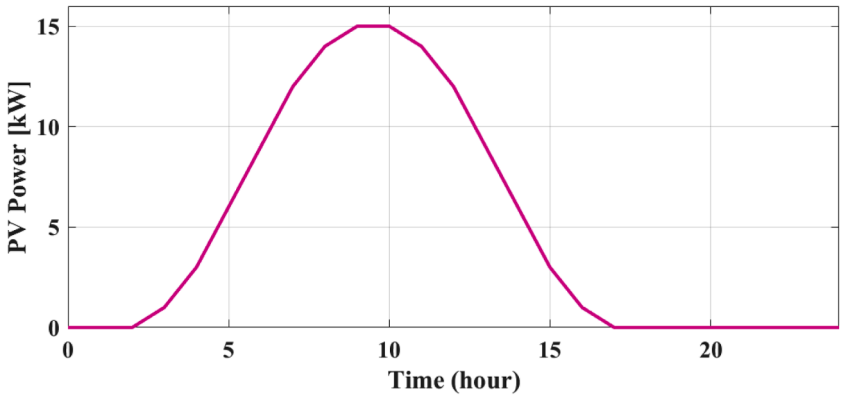

Fig. 8. Examination of PV power.

contributor when coupled with storage. Fig. 9 shows evaluation of SC power. The SC output remains mostly close to 0 kW throughout the day, with very small fluctuations between −1 kW and +1 kW. For example, minor peaks appear at around 2 kW at 8 h and again at 9 h, but values return near 0 kW quickly. This demonstrates the SC's role as a fast-response buffer, absorbing excess or providing short bursts to stabilize the DC bus without straining the battery. Fig. 10 illustrates evaluation of SoC. The SoC varies slightly between 84.3 % and 85.4 % across the full time span. At the start, the SoC is about 84.9 %, dips marginally to 84.6 % at 5 h, and then rises steadily, peaking at 85.4 % around 13 h. Afterward, it decreases to the lowest point of 84.3 % near 20 h, before climbing again towards 84.8 % by 24 h. This narrow band shows controlled charge–discharge cycles, preventing deep cycling and thereby prolonging battery life. The WbOA scheduler ensures balanced operation between SC and battery to maintain SoC stability. Fig. 11 shows evaluation of battery power. The battery begins with a charging state of around 2 kW at 0 h, increases to about 6 kW at 5 h, and then shifts into discharge mode, reaching −10 kW at 12 h. Following this, it recovers back to +6 kW at 18 h, stabilizing around 7 kW at 21 h, and then maintaining about 6 kW towards the end. This behaviour validates the role of the battery in long-duration energy shifting, unlike the SC which addresses short transients. Fig. 12 shows the convergence of WbOA. The convergence curve shows rapid improvement in early iterations and stabilization before the iteration limit. This demonstrates that WbOA avoids premature stagnation and efficiently finds near-global optima, validating its robustness for EM scheduling.

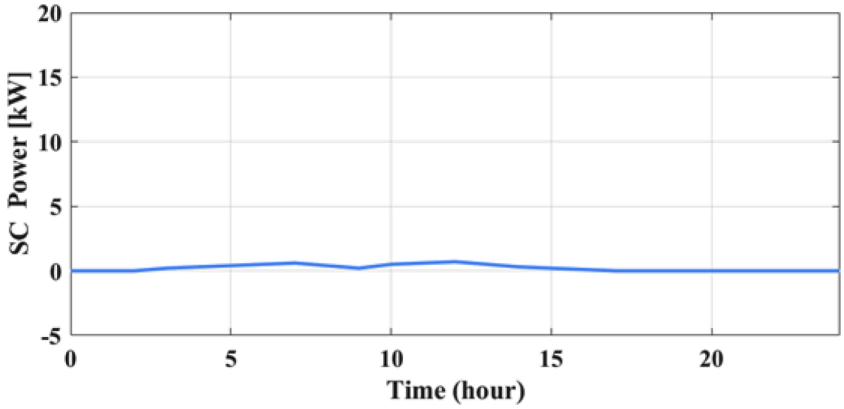

Fig. 9. Analysis of SC power.

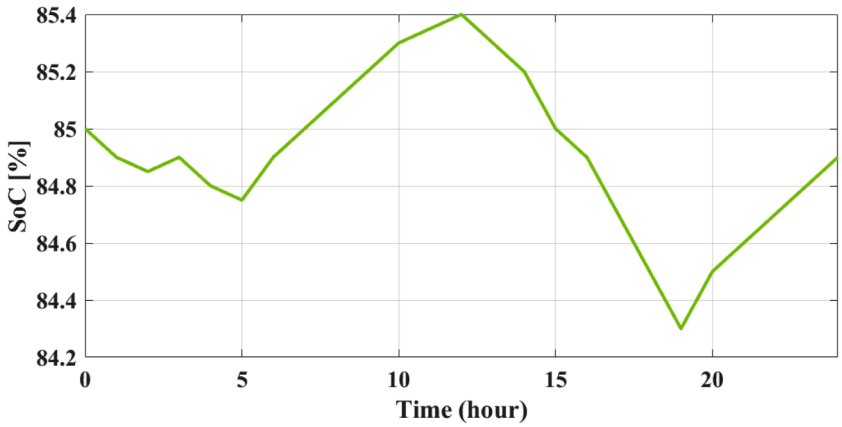

Fig. 10. Evaluation of SoC.

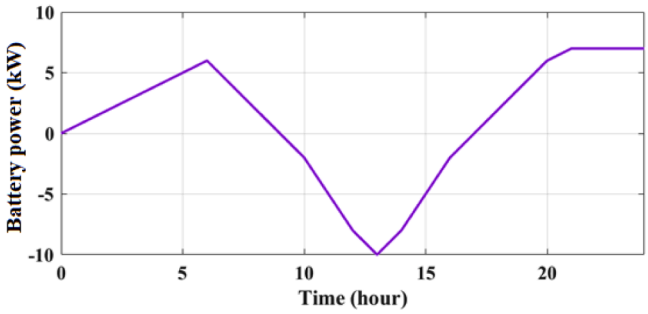

Fig. 11. Evaluation of battery power.

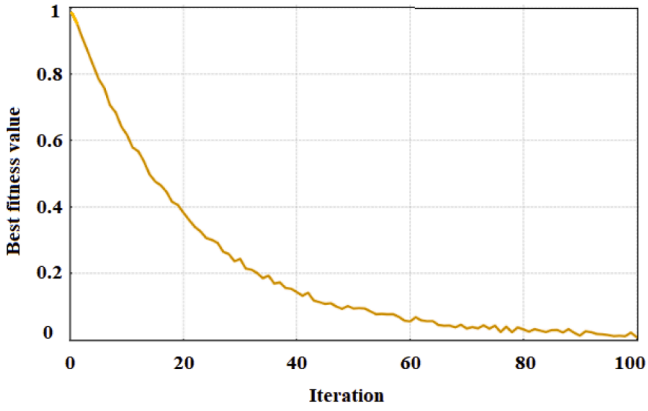

Fig. 12. Convergence of WbOA over iterations.

Table 4 provides a detailed comparison of the suggested WbOA-APINN method with existing methods. The WbOA-APINN records the best performance with an emission of 68 kg, operational cost of $124.5, efficiency of 98.7 %, and energy consumption of 1460 W. The PDO-MACNN method shows an emission of 75 ppm, cost of $135.2, efficiency of 96.7 %, and energy usage of 1510 W. The ANN method results in the highest emission of 94 ppm, the highest cost of $158.6, the lowest efficiency at 90.7 %, and the highest energy consumption of 1635 W. FFO-DADRCNN achieves 81 ppm emission, $140.4 cost, 92.6 % efficiency, and 1575 W energy use. MRA-FLC records 88 ppm emission, $149.8 cost, 93.4 % efficiency, and 1610 W energy consumption. Finally, CNN-ECOA shows 73 ppm emission, $137.9 cost, 91.3 % efficiency, and 1550 W energy usage. Competing methods such as ANN perform poorly due to limited adaptability, while hybrid methods like PDO-MACNN and CNN-ECOA perform moderately but are outperformed by the proposed approach. This proves the advantage of combining physics-informed forecasting with optimization.

The WbOA-APINN method requires slightly higher computational time compared to ANN, PDO-MACNN, and CNN-ECOA is shown in Table 5. This is primarily due to the integration of both optimization (WbOA) and physics-informed predictive modelling (APINN). However, the additional overhead remains acceptable, since MG EM typically operates on scheduling horizons (minutes to hours). Importantly, the improved operational cost reduction, emission minimization, and efficiency gains achieved by WbOA-APINN outweigh the marginal increase in computational demand.

Table 5
Computational time comparison of suggested and existing approaches.

Methods	Computational Time (s)	Relative Complexity	Remarks
ANN	4.2	Low	Fast convergence, but limited accuracy in prediction.
PDO-MACNN	7.9	Moderate	Additional complexity from multi-scale attention layers.
CNN-ECOA	8.4	Moderate–High	Optimization and CNN training increases overhead.
WbOA-APINN (proposed)	9.6	High	Higher due to joint optimization WbOA and APINN prediction, but justified by superior performance.

Table 4
Performance comparison of suggested and existing approaches.

Methods	CO_2 Emission (kg)	Operational cost ($)	Efficiency (%)	Energy Consumption (W)
WbOA-APINN	68	124.5	98.7	1460
PDO-MACNN	75	135.2	96.7	1510
ANN	94	158.6	90.7	1635
FFO-DADRCNN	81	140.4	92.6	1575
MRA-FLC	88	149.8	93.4	1610
CNN-ECOA	73	137.9	91.3	1550

Table 6
Statistical evaluation of algorithm performance (20 independent runs, mean ± standard deviation, with ANOVA and paired *t*-test results).

Metric	WbOA-APINN	PDO-MACNN	ANN	ANOVA *p*-value	WbOA-APINN vs. PDO-MACNN (*t*-test)
Operational Cost ($)	124.5 ± 1.8	136.2 ± 3.5	140.7 ± 2.9	< 0.01	$p = 0.003$
Efficiency (%)	98.7 ± 0.2	97.9 ± 0.4	97.5 ± 0.3	< 0.01	$p = 0.001$
Emissions (kg CO_2/kWh)	0.15 ± 0.01	0.21 ± 0.02	0.24 ± 0.02	< 0.01	$p = 0.004$

Table 6 presents the results of statistical significance testing based on 20 independent simulation runs. The values are reported as mean ± standard deviation for each metric. A one-way ANOVA test was first conducted across all methods, and the resulting p-values (< 0.01 for all metrics) confirm that the performance differences among the algorithms are statistically significant. To further validate the superiority of the suggested WbOA-APINN approach, paired *t*-tests were performed against PDO-MACNN, which was identified as the best-performing competitor in Table 2. The results show that WbOA-APINN achieves significantly lower operational cost ($p = 0.003$), higher efficiency ($p = 0.001$), and reduced emissions ($p = 0.004$) at the 95 % confidence level. These findings confirm that the improvements reported in Table 4 are not due to random variation but are statistically robust, thereby reinforcing the effectiveness of WbOA-APINN.

4.1. Discussion

The suggested WbOA-APINN framework was evaluated in a renewable-integrated MG with hybrid storage under realistic PV, wind, and demand profiles. The results confirm effective coordination of renewable sources, storage units, and the grid. The SC primarily handled short bursts to smooth fluctuations, while the battery managed deeper charge–discharge cycles with a stable SoC, ensuring extended lifetime. Grid interaction balanced variability, and the convergence characteristics of WbOA demonstrated rapid and stable optimization. Compared with benchmark methods, WbOA-APINN consistently achieved lower emissions, reduced operational cost, and higher efficiency. Although computational time was slightly higher than simpler models, it remained well within practical limits for MG scheduling horizons. Statistical validation across multiple runs confirmed the robustness of improvements. These findings demonstrate that integrating WbOA with APINN provides reliable forecasting, efficient scheduling, and tangible economic and environmental benefits. Unlike standalone ANN, which showed poor adaptability due to its reliance on data alone, or simpler heuristic methods limited by convergence issues, WbOA-APINN ensures optimal power distribution and enhanced renewable utilization, making it highly suitable for sustainable MG operation.

5. Conclusion

This manuscript suggests high-performance method for intelligent EM in MG systems integrated with RESs and HESS using the WbOA-APINN technique. The suggested method achieves outstanding results, recording a minimum emission of 68 ppm, a reduced operational cost of $124.5, high efficiency of 98.7 %, and the lowest energy consumption of 1460 W. Compared to existing methods such as PDO-MACNN (75 ppm, $135.2, 96.7 %, 1510 W), ANN (94 ppm, $158.6, 90.7 %, 1635 W), FFO-DADRCNN (81 ppm, $140.4, 92.6 %, 1575 W), MRA-FLC (88 ppm, $149.8, 93.4 %, 1610 W), and CNN-ECOA (73 ppm, $137.9, 91.3 %, 1550 W), the WbOA-APINN method outperforms in all key metrics. Simulation results validate its ability to optimize power distribution, manage hybrid ES scheduling, and forecast renewable generation and load demand under varying conditions. Overall, WbOA-APINN enhances system responsiveness, lowers environmental impact, and ensures effective and reliable energy flow in MGs with renewable integration.

5.1. Future works

While this study validated the suggested WbOA-APINN framework on a single-area MG, several promising extensions remain. Future research will focus on integrating demand response and EVC as additional decision variables to enhance flexibility, extending the framework to larger multi-area and cluster-based MGs with heterogeneous resources, and explicitly modelling uncertainties such as sensor failures, measurement errors, and communication delays to improve robustness. Moreover, incorporating detailed voltage and frequency stability constraints consistent with IEEE grid codes and adopting advanced electrochemical degradation models for batteries and SCs will provide more accurate lifetime assessment. These extensions will strengthen the scalability, practicality, and resilience of the framework for deployment in next-generation smart MGs.

CRediT authorship contribution statement

Jegadeesh Kumar R: Writing – review & editing, Validation, Investigation, Formal analysis, Conceptualization. **Vijayakumar P:** Writing – review & editing, Validation, Supervision, Project administration, Conceptualization. **Santhosh Paramasivam:** Writing – review & editing, Validation, Investigation, Formal analysis, Conceptualization. **Amit Kumar:** Writing – review & editing, Visualization, Validation. **Gianluca Gatto:** Writing – review & editing, Visualization, Validation, Supervision, Project administration.

Declaration of competing interest

The authors declare that they have no known competing financial interests or personal relationships that could have appeared to influence the work reported in this paper.

Data availability

No data was used for the research described in the article.

References

[1] M.B. Abdelghany, A. Al-Durra, F. Gao, A coordinated optimal operation of a grid-connected wind-solar microgrid incorporating hybrid energy storage management systems, IEEe Trans. Sustain. Energy 15 (1) (2023) 39–51.
[2] H.M. Mohan, S.K. Dash, Renewable energy-based DC microgrid with hybrid energy management system supporting electric vehicle charging system, Systems 11 (6) (2023) 273. . *(Basel)*.
[3] Y. Belkhier, A. Oubelaid, Novel design and adaptive coordinated energy management of hybrid fuel-cells/tidal/wind/PV array energy systems with battery storage for microgrids, Energy Storage 6 (1) (2024) e556.
[4] C.J. Jena, P.K. Ray, Power management in three-phase grid-integrated PV system with hybrid energy storage system, Energies 16 (4) (2023) 2030. . *(Basel)*.
[5] D. Yousri, H.E. Farag, H. Zeineldin, E.F. El-Saadany, Integrated model for optimal energy management and demand response of microgrids considering hybrid hydrogen-battery storage systems, Energy Convers. Manage 280 (2023) 116809.
[6] A.M. Adeyinka, O.C. Esan, A.O. Ijaola, P.K. Farayibi, Advancements in hybrid energy storage systems for enhancing renewable energy-to-grid integration, Sustain. Energy Res. 11 (1) (2024) 26.
[7] H. Abouobaida, L. de Oliveira-Assis, E.P. Soares-Ramos, H. Mahmoudi, J. M. Guerrero, M. Jamil, Energy management and control strategy of DC microgrid based hybrid storage system, Simul. Model. Pract. Theory 124 (2023) 102726.
[8] C. Álvarez-Arroyo, S. Vergine, A.S. de la Nieta, L. Alvarado-Barrios, G. D'Amico, Optimising microgrid energy management: leveraging flexible storage systems and full integration of renewable energy sources, Renew. Energy 229 (2024) 120701.
[9] C.B. Ndeke, M. Adonis, A. Almaktoof, Energy management strategy for a hybrid micro-grid system using renewable energy, Discover Energy 4 (1) (2024) 1.
[10] S. Patel, A. Ghosh, P.K. Ray, V. Gurugubelli, Effective power management strategy and control of a hybrid microgrid with hybrid energy storage systems, IEEe Trans. Ind. Appl. 59 (6) (2023) 7341–7355.

[11] M. Talaat, M.H. Elkholy, A. Alblawi, T. Said, Artificial intelligence applications for microgrids integration and management of hybrid renewable energy sources, Artif. Intell. Rev. 56 (9) (2023) 10557–10611.
[12] S.M. Abu, M.A. Hannan, S.A. Rahman, C.Y. Long, P.J. Ker, R.T. Wong, G. Jang, An effective optimization algorithm for hydrogen fuel cell-based hybrid energy system: a sustainable microgrid approach, Int. J. Hydrogen Energy 98 (2025) 1341–1355.
[13] F. Moazzen, M.J. Hossain, A two-layer strategy for sustainable energy management of microgrid clusters with embedded energy storage system and demand-side flexibility provision, Appl. Energy 377 (2025) 124659.
[14] O. Ibrahim, M.J.A. Aziz, R. Ayop, A.T. Dahiru, W.Y. Low, M.H. Sulaiman, T. I. Amosa, Fuzzy logic-based particle swarm optimization for integrated energy management system considering battery storage degradation, Results Eng. 24 (2024) 102816.
[15] H. Karimi, S. Jadid, S. Hasanzadeh, Optimal-sustainable multi-energy management of microgrid systems considering integration of renewable energy resources: a multi-layer four-objective optimization, Sustain. Prod. Consum. 36 (2023) 126–138.
[16] R. Sathishkumar, M. Venkateswaran, P. Deepamangai, P. Soundar Rajan, An efficient power management control strategy for grid-independent hybrid renewable energy systems with hybrid energy storage: hybrid approach, J. Energy Storage 96 (2024) 112685.
[17] S.K. Ramu, I. Vairavasundaram, B. Palaniyappan, A. Bragadeshwaran, B. Aljafari, Enhanced energy management of DC microgrid: artificial neural networks-driven hybrid energy storage system with integration of bidirectional DC-DC converter, J. Energy Storage 88 (2024) 111562.
[18] M.J. Kumar, T. Sampradeepraj, E. Sivajothi, G. Singh, An efficient hybrid technique for energy management system with renewable energy system and energy storage system in smart grid, Energy 306 (2024) 132454.
[19] O. Chekira, Y. Boujoudar, H. El Moussaoui, A. Boharb, T. Lamhamdi, H. El Markhi, An improved microgrid energy management system based on hybrid energy storage system using ANN NARMA-L2 controller, J. Energy Storage 98 (2024) 113096.
[20] S. Sruthi, K. Karthikumar, P. Chandrasekhar, An efficient power management control strategy for grid-independent hybrid renewable energy systems with hybrid energy storage: hybrid approach, J. Energy Storage 95 (2024) 112325.
[21] D. Srikanth, G.D. Sukumar, P.V. Sobhan, A convolutional neural network based energy management system for photovoltaic/battery systems in microgrid using enhanced coati optimization approach, J. Energy Storage 119 (2025) 116252.
[22] A.S. Alghamdi, Microgrid energy management and scheduling utilizing energy storage and exchange incorporating improved gradient-based optimizer, J. Energy Storage 97 (2024) 112775.
[23] R.P. Kumar, G. Karthikeyan, A multi-objective optimization solution for distributed generation energy management in microgrids with hybrid energy sources and battery storage system, J. Energy Storage 75 (2024) 109702.
[24] A. Merabet, A. Al-Durra, E.F. El-Saadany, Energy management system for optimal cost and storage utilization of renewable hybrid energy microgrid, Energy Convers. Manage 252 (2022) 115116.
[25] T. Hai, N.S.S. Singh, F. Jamal, Energy management of a microgrid with integration of renewable energy sources considering energy storage systems with electricity price, J. Energy Storage 110 (2025) 115191.
[26] M. Manikandan, R. Saravanan, G. Kannayeram, M. Saravanan, Integrating renewable resources and electric vehicles: an approach for effective energy management in DC microgrid, Sol. Energy 299 (2025) 113775.
[27] N.C. Gaitan, I. Ungurean, G. Corotinschi, C. Roman, An intelligent energy management system solution for multiple renewable energy sources, Sustainability 15 (3) (2023) 2531.
[28] Y. Belkhier, M.D. Alshehri, R.N. Shaw, A. Ghosh, An intelligent energy management system of hybrid solar/wind/battery power sources integrated in smart DC microgrid for smart university. Applications of AI and IOT in Renewable Energy, Academic Press, 2022, pp. 57–88.
[29] D. Carrasco-Gonzalez, R. Sarrias-Mena, P. Horrillo-Quintero, F. Llorens-Iborra, L. M. Fernandez-Ramirez, Design and raspberry Pi-based implementation of an intelligent energy management system for a hybrid AC/DC microgrid with renewable energy, battery, ultracapacitor and hydrogen system, Comput. Electr. Eng. 123 (2025) 110253.
[30] K. Shafiei, A. Seifi, M.T. Hagh, A novel multi-objective optimization approach for resilience enhancement considering integrated energy systems with renewable energy, energy storage, energy sharing, and demand-side management, J. Energy Storage 115 (2025) 115966.
[31] E.N. Nyeche, E.O. Diemuodeke, Modelling and optimisation of a hybrid PV-wind turbine-pumped hydro storage energy system for mini-grid application in coastline communities, J. Clean. Prod. 250 (2020) 119578.
[32] V. Mounica, Y.P. Obulesu, Hybrid power management strategy with fuel cell, battery, and supercapacitor for fuel economy in hybrid electric vehicle application, Energies 15 (12) (2022) 4185. . *(Basel)*.
[33] W. Long, T. Wu, M. Xu, M. Tang, S. Cai, Parameters identification of photovoltaic models by using an enhanced adaptive butterfly optimization algorithm, Energy 229 (2021) 120750.
[34] B. Sun, A multi-objective optimization model for fast electric vehicle charging stations with wind, PV power and energy storage, J. Clean. Prod. 288 (2021) 125564.
[35] A. Elnozahy, A.M. Yousef, S.S. Ghoneim, S.A.M. Abdelwahab, M. Mohamed, F. K. Abo-Elyousr, Optimal economic and environmental indices for hybrid PV/wind-based battery storage system, J. Electr. Eng. Technol. 16 (6) (2021) 2847–2862.
[36] A.A. Al Alahmadi, Y. Belkhier, N. Ullah, H. Abeida, M.S. Soliman, Y.S.H. Khraisat, Y.M. Alharbi, Hybrid wind/PV/battery energy management-based intelligent non-integer control for smart DC-microgrid of smart university, IEEe Access. 9 (2021) 98948–98961.
[37] Z. Benmamoun, K. Khlie, M. Dehghani, Y. Gherabi, WOA: wombat optimization algorithm for solving supply chain optimization problems, Mathematics 12 (7) (2024) 1059.
[38] Z. Hu, A.D. Jagtap, G.E. Karniadakis, K. Kawaguchi, Augmented Physics-Informed Neural Networks (APINNs): a gating network-based soft domain decomposition methodology, Eng. Appl. Artif. Intell. 126 (2023) 107183.